Dalton Transactions

Accepted Manuscript

ROYAL SOCIETY OF CHEMISTRY

www.rsc.org/dalton

Journal Name

RSCPublishing

ARTICLE

Controllable synthesis of Ni/SiO_2 hollow spheres and excellent catalytic performance in 4-nitrophenol reduction

Cite this: DOI: 10.1039/x0xx00000x

Received 00th January 2012,
Accepted 00th January 2012

DOI: 10.1039/x0xx00000x

www.rsc.org/

Zhongyi Niu,[a,b] Shenghuan Zhang,[a,b] Yanbo Sun,*[c] Shili Gai,[a] Fei He,[a] Yunlu Dai,[a] Lei Li,[a] and Piaoping Yang*[a]

The high cost of noble metal nanoparticles used for catalytic reduction of 4-nitrophenol (4-NP) leads to the extensive study of Ni nanoparticles (NPs) for their low cost and magnetic properties. However, the conventional routes of preparing the ferromagnetic Ni NPs usually lead to large particle size and aggregation. In this study, we propose a simple two-step method for the synthesis of hierarchical Ni NPs supported silica magnetic hollow microspheres (Ni/SiO_2 MHMs). Tiny Ni NPs are well dispersed on the supports with high loading amounts (15 wt. %). The size of Ni NPs can be tuned from 10 nm to 21 nm with the size of Ni/SiO_2 MHMs increasing from 230 nm to 800 nm. The as-prepared samples exhibit excellent catalytic activity in the reduction of 4-NP. Furthermore, the experimental results prove the size of Ni NPs plays an important role in the catalytic activity. The catalytic activity of small size Ni NPs is higher than that of large size and many other supported Ni NPs catalysts as reported. In particular, the magnetic property of Ni/SiO_2 MHMs makes it easy to recycle for reuse.

1. Introduction

4-Aminophenol (4-AP) is an important chemical intermediate for synthesizing analgesic and antipyretic drugs, dyestuffs and photographic developers, corrosion inhibitor, anticorrosion lubricant, and so on.[1] Nowadays, the production of 4-AP is mainly through catalytic hydrogenation of 4-nitrophenol using noble metal (e.g. Pt, Au, Ag and Pd) catalysts.[2–7] This reaction is very environmental friendly because 4-NP widely exist in industrial waste water. However, the disadvantage of this process is the high cost of the used noble metal catalysts. An alternative green process is catalytic reduction of 4-NP by transition metal.[8–10] Especially, the combination of catalytic and magnetic properties makes nickel based catalysts be popular in the area of catalysts.[11–13]

With the advances in materials science, much attention has been focused on nanomaterials for their unusual electronic, optical, magnetic and chemical properties which are significantly different from those of the bulk materials.[14–16] However, except for the advantage arising from the small size, aggregation will take place due to the large surface area-to-volume.[17] In order to avoid aggregation, the common method is to immobile the nanoparticles (NPs) on a solid support. So far, various supports have been used for immobilizing NPs such as porous carbon, hollow silica, graphene oxide, and mesoporous silica.[18–21] In addition, multifunctional supports such as magnetic supports are also very popular.[22] However, finding a suitable support and immobilizing the NPs on the support with highly dispersion is of great challenge.

An ideal support material should possess the characteristics such as high surface area, high inertness in harsh condition and low cost. Hollow nanomaterials are the most promising candidate, owing to their potential application in catalysts, drug delivery, electrochemistry and bio-imaging.[23–26] As a special branch of hollow micro/nanomaterials, multilevel (hierarchical) hollow nanomaterials which are composed of nanosheets, nanowires or nanotubes have been extensively pursued in recent years due to their high surface area.[27–29] Two methodologies have been developed to fabricate this kind of hollow nanomaterials: one is template approach which includes hard-templating method (e.g., carbon, silica and metal oxide spheres)[30–32] and soft-templating method (e.g. supramolecular assemblies of surfactant and polymer).[33–35] And the other is template-free approach which is mainly based on kirkendall effects and Ostwald ripening.[36–39] Different from template synthetic routes, which require calcination or etching to remove the templates, this is a facile, one-step solution for the preparation of inorganic hollow nanostructures. However, in general, it remains a great challenge to immobilize the NPs on the hierarchical hollow support with large loading amount.

In this paper, uniform Ni NPs supported silica magnetic hollow microspheres (Ni/SiO_2 MHMs) were prepared by a simple two-step methods. That is a simple hydrothermal method based on Kirkendall effects which was carried out to fabricate hollow nickel silicate precursor and then an *in situ* thermal decomposition and reduction method was used to obtain the final products. The Ni/SiO_2 MHMs with a controllable diameter (230 nm to 810 nm) could be easily obtained by adjusting the size of silicate precursor. And the size of Ni NPs is closely related to the size of Ni/SiO_2 MHMs. The advantages of this unique synthetic method are facility and the Ni NPs have ultra-small particle size, high Ni loading amount

and good dispersion. Comparing to other conventional loading method, the NPs can bind to the support more firmly and uniformly. Furthermore, the size of Ni nanoparticles is controllable. The Ni/SiO_2 MHMs was employed as catalyst to investigate the catalytic performance in reduction of 4-NP, and the stability of the multifunctional catalyst was also studied.

2. Experimental section

2.1. Reagents and Materials

Tetraethyl orthosilicate (TEOS), nickel chloride, ammonium chloride, concentrated ammonia solution (25-28 wt. %), $NaBH_4$, and 4-NP are of analytical grade and were all purchased from Sinopharm Chemical Reagent Co., Ltd. (China). All chemicals are of analytical grade and used without further purification.

2.2. Synthesis

Synthesis of silica microspheres: Monodisperse silica microspheres with particles size of 140 nm, 210 nm, 350 nm and 580 nm were prepared by hydrolysis of tetraethyl orthosilicate (TEOS) in an alcohol medium containing water and ammonia *via* a typical Stöber process.[40] The size of the particles dependeds on the relative concentration of the reactants. The experimental conditions for obtaining the SiO_2 particles with size of 140, 210, 350 and 580 nm are list in Table S1, which are denoted as SiO_2-A, SiO_2-B, SiO_2-C, SiO_2-D, respectively. In a typical hydrolysis process, the mixture containing H_2O, alcohol, ammonia and TEOS was stirring for 5 h at room temperature. The SiO_2 particles are centrifugally separated from the white silica colloidal suspension and then washed with ethanol for four times.

Synthesis of hollow nickel silicate precursor: Monodisperse hollow nickel silicate precursors were prepared *via* simple hydrothermal method. The mixture of 0.75 mmol nickel chloride and 10 mmol ammonia chloride was dissolved in 20 mL deionized (DI) water to form a clear solution. Then 1 mL ammonia solution was added to the solution under stirring. The solution turned from light green to deep blue immediately. 100 mg as-prepared SiO_2 particles was dispersed in 10 mL deionized water and ultrasound for 20 min. The above two solutions were mixed under ultrasonication and then transferred into an autoclave (40 mL), heated to 100 °C and kept for 12 h. After the autoclave was cooled to room temperature, the resulting light green precipitates were collected and washed several times with distilled water and absolute ethanol. The final products were dried at 60 °C for 12 h.

Synthesis of Ni/SiO_2 MHMs: Ni/SiO_2 MHMs were prepared through an *in situ* thermal decomposition and reduction method. 100 mg nickel silicate precursor was placed in a ceramic boat in the middle of the horizontal tube furnace. The final products were collected in the ceramic boat at room temperature after heating at 800 °C for 7 h in 5% H_2/N_2 gas.

2.3. Catalytic reaction

The reduction of 4-NP by $NaBH_4$ was chosen as a typical reaction to investigate the catalytic performance of Ni/SiO_2 MHMs with different sizes. A total of 1 mL of sodium borohydride solution (0.2 mol/L) was added into a light yellow solution containing 100 μL 4-NP (5 mmol/L) and 2 mL deionized water. After that, 3 mg of Ni/SiO_2 MHMs catalysts was added. After the immediate addition of the catalysts, UV spectra of the sample were taken every 3 min in the range of 250-500 nm. The rate constant of the reaction was determined by measuring the change in intensity of the peak at 400 nm with time. The catalytic activity affected by the size of Ni NPs is investigated through this way.

2.4. Characterization

X-ray diffraction (XRD) measurement was examined on a Rigaku D/max-TTR-III diffractometer using monochromatic Cu Kα radiation (λ = 0.15405 nm). The morphologies of the samples were inspected on a scanning electron microscope (SEM, Hitachi S-4800). Transmission electron microscopy (TEM) images and high resolution TEM (HRTEM) were obtained with a FEI Tecnai G^2 S-Twin transmission electron microscope with a field emission gun operating at 200 kV. Images were acquired digitally on a Gatan multiple CCD camera. Specific surface areas of the samples were determined using N_2 adsorption-desorption isotherms at 77 K (Micromeritics TriStar II 3020) with Brunauer-Emmett-Teller (BET) method. Inductively coupled plasma (ICP) analysis (Thermo iCAP 6000 ICPOES) were used to measure the elemental composition of the above studied samples. Magnetization measurements were performed on a MPM5-XL-5 superconducting quantum interference device (SQUID) magnetometer at 300 K. The absorbance of 4-NP was obtained on a UV-vis spectrophotometer (TU-1901).

3. Results and discussion

3.1. Characterization of Ni/SiO_2 MHMs with different size

Scheme 1 shows the typical synthetic steps for the preparation of Ni/SiO_2 MHMs, starting from silica which is synthesized through classical Stöber method. Under alkaline condition at high temperature, the silica chains on the surface of colloidal silica will be broken by hydroxide, resulting in the generation of silicate ions. Nickel silicate is formed *in situ* around the silica cores when the silicate ions directly react with nickel ions. Then the inner colloidal silica will go on dissolving into silicate ions following the formation of nickel silicate until the silica core was dissolved completed.[41] The final Ni/SiO_2 MHMs will be obtained by thermal decomposition at high temperature and reduction under H_2 *in situ*.

The XRD pattern (Fig. S1) of the light green power obtained by hydrothermal reaction can be indexed to nickel silicate hydrates, which are poorly crystalline. The EDS spectrum (Fig. S2) indicates the existence of Ni, Si, and O elements in the sample while C element is from the conducting resin. After decomposition and reduction, the XRD diffractions (Fig. 1) of the all the samples with different sizes are given in Fig. 1. The three peaks centered at 2θ values of 44.5°, 51.8°, and 76.4° can be assigned to the reflections of the (111), (200), and (220) crystalline planes of cubic-phased Ni (JCPDS No. 04–0850), respectively. And no other phases can be detected except for a low broad band at 2θ = 22° assigned to amorphous silica, indicating that nickel silicate hydrates precursor has been converted to cubic-phased Ni and amorphous silica completely. Furthermore, the relatively broad

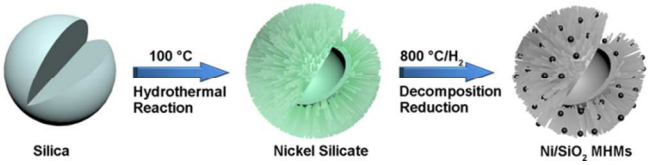

Scheme 1 Schematic illustration of the synthetic procedure for Ni/SiO_2 MHMs.

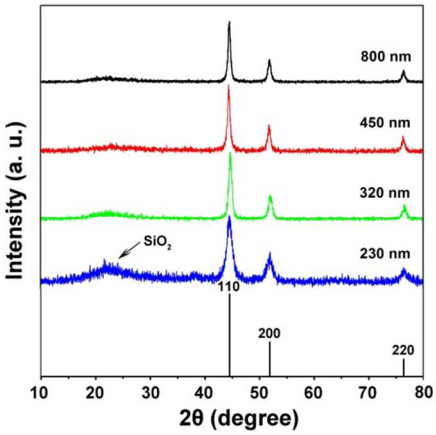

Fig. 1 XRD pattern of Ni/SiO_2 MHMs.

peaks of Ni indicate the nano-sized nature of Ni NPs in the composite.

The SEM images of monodispersed silica colloid particles with tunable size are displayed in Fig. 2A1, B1, C1 and D1. Clearly, the silica all consist of uniform spheres with a mean diameter of 140 nm, 230 nm, 350 nm and 580 nm, respectively. Fig. 2A2, B2, C2 and D2 show the corresponding nickel silicate precursors obtained after hydrothermal reaction using the silica templates previous synthesized. Comparing to the silica template, the surface of nickel silicate is rougher. Moreover, numerous uniform petal-like unites are formed. And the insets in Fig. 2A2, B2, C2 and D2 show the petal-like units are very thin nanosheets. The size of the nickel silicate is larger than that of silica template. And it is measured to be 230 nm, 320 nm, 450 nm and 800 nm, which increases 90 nm, 90 nm, 100 nm and 230 nm respectively compared to silica templates. As for Ni/SiO_2, the size and spherical structures can still be observed in Fig. 2A3, B3, C3 and D3, indicating that high temperature has little influence on the shape and size. Notably, the insets in

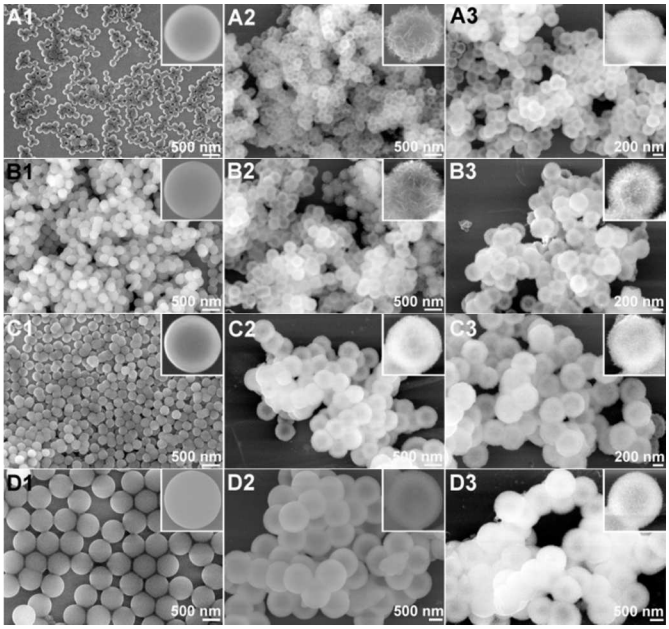

Fig. 2 SEM images of SiO_2-A (A1), $NiSiO_3$ (A2), Ni/SiO_2 MHMs (A3); SiO_2-B (B1), $NiSiO_3$ (B2), Ni/SiO_2 MHMs (B3); SiO_2-C (C1), $NiSiO_3$ (C2), Ni/SiO_2 MHMs (C3); SiO_2-D (D1), $NiSiO_3$ (D2), Ni/SiO_2 MHMs (D3).

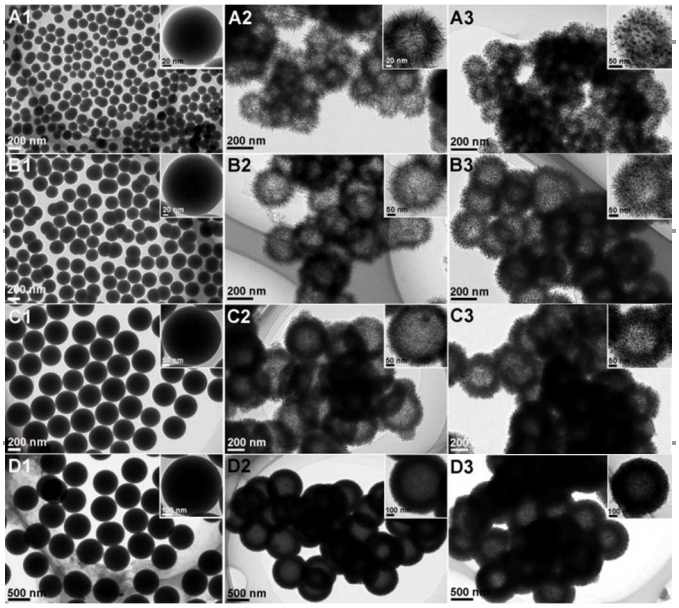

Fig. 3 TEM images of SiO_2-A (A1), $NiSiO_3$ (A2), Ni/SiO_2 MHMs (A3); SiO_2-B (B1), $NiSiO_3$ (B2), Ni/SiO_2 MHMs (B3); SiO_2-C (C1), $NiSiO_3$ (C2), Ni/SiO_2 MHMs (C3); SiO_2-D (D1), $NiSiO_3$ (D2), Ni/SiO_2 MHMs (D3).

Fig. 2A3, B3, C3 and D3 show numerous tiny particles on the surface besides thin nanaosheets, indicating the generation of Ni NPs.

The structure of the sample was further investigated by TEM images in Fig. 3. We can see that well dispersed SiO_2 colloid particles with different size are obtained (Fig. 3A1, B1, C1, and D1). It can be clearly seen the hollow structure of nickel silicate in Fig 3A2, B2, C2, and D2. The respective shell is determined to be about 70 nm, 80 nm, 110 nm and 180 nm in thickness. And the size and shape of all Ni/SiO_2 MHMs (Fig. 3A3, B3, C3

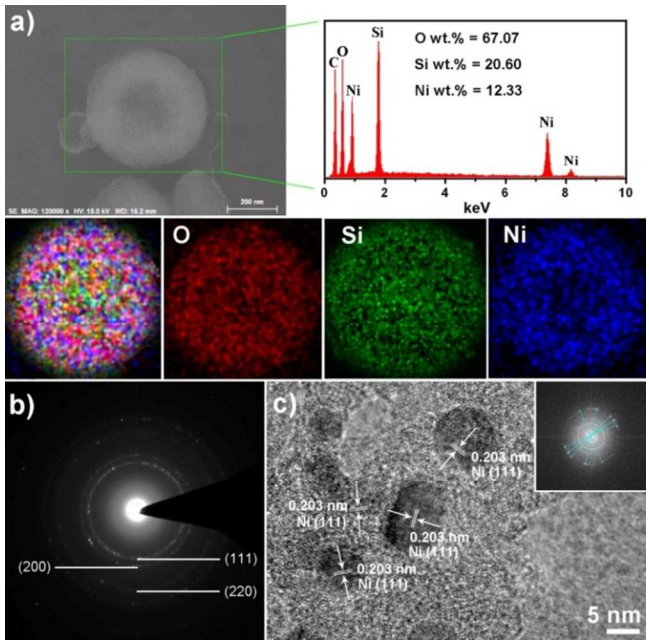

Fig. 4 a) EDS and element mapping of Ni/SiO_2 MHMs, b) SAED pattern, and c) HRTEM image (inset is corresponding FFT pattern).

and D3) keeps in accordance with the SEM images (Fig. 2). Additionally, numerous tiny Ni NPs can be clearly seen in Fig. 3A3, B3, C3 and D3. The size distribution of Ni NPs (Fig. S4), which is calculated from insets of Fig. 3A3, B3, C3 and D3, shows that the size of Ni NPs is mainly centred at 10–13 nm, except for the 800 nm Ni/SiO_2 MHMs which is centred at 21 nm. Therefore, there is a general tendency that the size of Ni NPs will become larger with the increase of Ni/SiO_2 MHMs. It is worthwhile to notice that Ni NPs are nearly monodisperse which suggests that this *in situ* calcination and reduction method is efficient in preventing aggregation of Ni NPs. Fig. S3 shows the XRD pattern of sample calcined in the air for at 800 °C 8 h, which can be indexed to rhombohedral phased NiO (JCPDS No. 44–1159). Therefore, the *in situ* calcination and reduction process can be considered as two steps: nickel silicate hydrate is firstly decomposed into nickel oxide, and then the reduction process converts NiO into Ni NPs. In this way, Ni NPs can be attached on the lamellar structured silica more firmly because of the continuous process. Thus, aggregation is avoided to a large degree eventually. It is well accepted the catalytic activity of the catalyst is affected by the size of active Ni NPs, which will be discussed later.

The Ni/SiO_2 MHMs were also examined by the EDS (Fig. 4a) which show the existence of Ni, Si, and O elements (the C element is ascribed to carbon carbon conductive tape). It is clear that high loading amount of Ni (about 12 wt. %) has been achieved. Additionally, the elemental mapping of the SEM image reveals the elements of Ni, Si and O are uniformly dispersed on the shell. The high dispersion and high loading amount can be due to the unique *in situ* thermal decomposition and reduction process. Fig. 4b displays the selected area electron diffraction (SAED) pattern of Ni/SiO_2 MHMs. It shows three rings and the interplanar spacing is calculated to be

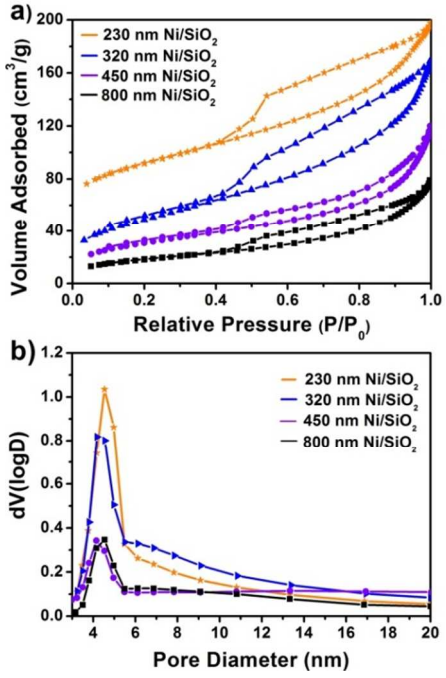

Fig. 5 N_2 adsorption/desorption isotherms of Ni/SiO_2 MHMs with different size (a) and their corresponding pore size distributions (b).

Table 1 The BET surface area, total pore volume, and average pore size of Ni/SiO_2 MHMs with different diameters.

	BET surface area (m^2/g)	Pore volume (cm^3/g)	Average pore size (nm)
230 nm Ni/SiO_2	185	0.26	5.85
320 nm Ni/SiO_2	177	0.24	6.36
450 nm Ni/SiO_2	111	0.18	7.17
800 nm Ni/SiO_2	65	0.12	7.99

0.20 nm, 0.17 nm and 0.12 nm, which correspond to the (111), (200) and (220) crystalline planes of cubic nickel, respectively. And the results also match well with the XRD results in Fig. 1. Fig. 4c shows that the adjacent lattice fringes (marked by the arrows) are determined to be about 0.20 nm, which correspond well to the d_{111} spacing of cubic Ni (JCPDS No. 04–0850). Inset in Fig. 4c is its corresponding FFT pattern, and any pairs of diffraction spots can be calculated to the (111) plane of cubic Ni (the corresponding interplanar spacing is 0.2 nm).

N_2 adsorption/desorption isotherms of Ni/SiO_2 MHMs with different sizes are displayed in Fig. 5a. All of the samples can be classified to type-IV isotherms with hysteresis loop, indicating the presence of mesopores. The corresponding pore size distributions are displayed in Fig. 5b. Table 2 summarizes the textural parameters of the samples with different sizes. It is obvious that when the size of Ni/SiO_2 MHMs increases from 230 nm to 800 nm, the BET surface area decreases from 185 m^2/g to 65 m^2/g, and the average pore size increases from 5.85 nm to 7.99 nm. The large surface area suggests its potential application in catalytic reaction and it will be discussed in the following section.

Fig. 6 shows the magnetization curves of Ni/SiO_2 MHMs with different size at 300 K. The range of magnetization saturation (Ms) value is from 8.9 emu/g to 19.9 emu/g. And it is obvious that there is no significant coercivity or remanence of all the samples in Fig. 6. The enlarged magnetization curve of 230 nm Ni/SiO_2 MHMs (Inset Fig. 6) shows the coercivity is 15 Oe which indicates the sample is very close to superparamagnetic state. And it can well describe the magnetic-recyclability of the samples. In current case, the as-prepared Ni/SiO_2 MHMs can quickly respond to an external magnetic field after dispersing in water (Fig. S5), made it possible to be recycled for reuse.

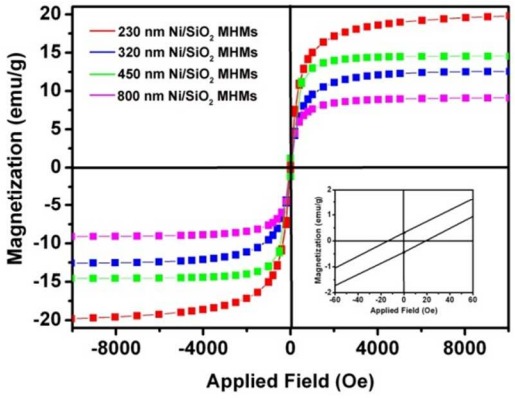

Fig. 6 Magnetization curves of Ni/SiO_2 MHMs at room temperature. The inset is the enlargement magnetization curves of 230 nm Ni/SiO_2 MHMs near origin (low right).

3.2. Catalytic performance of Ni/SiO_2 MHMs with different size

The catalytic performance of Ni/SiO_2 MHMs with different size was evaluated by the model reaction of the reduction of 4-NP

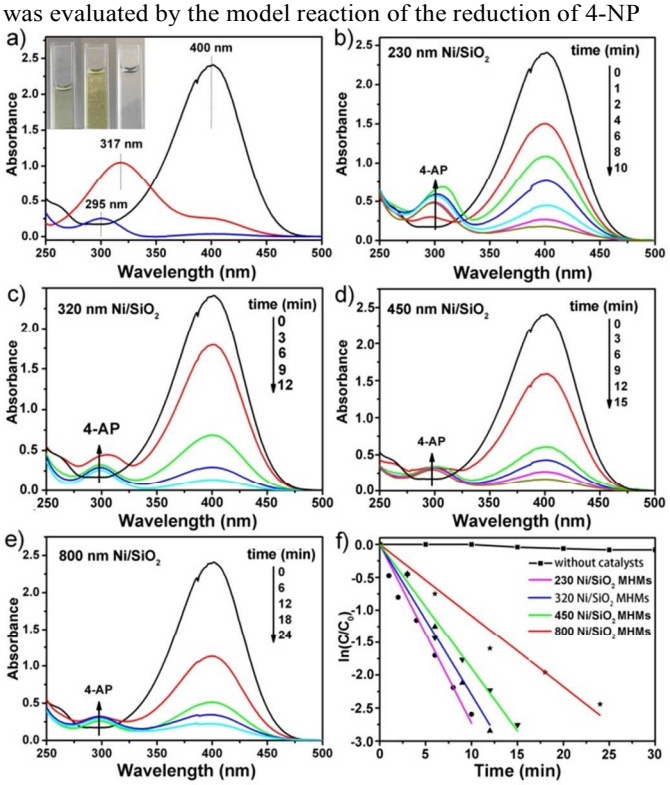

Fig. 7 a) UV-vis absorption spectra of 4-AP and 4-NP before and after adding NaBH4; b) successive reduction of 4-NP using 230 nm Ni/SiO_2 MHMs as catalysts; c) successive reduction of 4-NP using 350 nm Ni/SiO_2 MHMs as catalysts; d) successive reduction of 4-NP using 500 nm Ni/SiO_2 MHMs as catalysts; e) successive reduction of 4-NP using 800 nm Ni/SiO_2 MHMs as catalysts; f) $\ln(C/C_0)$ verse reaction time for the reduction of 4-NP over different sizes of Ni/SiO_2 MHMs. The ratio of 4-NP concentration (C_t at time t) to its initial value C_0 is directly represented by the relative intensity of the respective absorption peak at 400 nm.

with excess aqueous $NaBH_4$ solution at room temperature.[42] In Fig. 7a, the absorption peaks centered at 317 nm, 400 nm and 295 nm are assigned to the characteristic absorption of 4-NP, 4-nitrophenolate generated after adding aqueous $NaBH_4$ and 4-AP, respectively.[43] And the change of the corresponding color is displayed inside Fig. 7a, which is light yellow, bright yellow and colorless, respectively. Fig. 7b-e present the UV-vis spectra of the 4-NP monitored at different time for the whole reduction process. It is clear that the peak centered at 400 nm gradually disappears and a new peak centered at 295 nm appears. The full reduction of 4-NP by $NaBH_4$ are completed within 10 min, 12 min, 15 min and 24 min by using 230 nm, 350 nm, 450 nm and 800 nm Ni/SiO_2 MHMs as catalysts, respectively. Since the concentration of $NaBH_4$ greatly exceeds that of 4-NP (C_{NaBH4} : $C_{4\text{-}NP}$ = 400 : 1), the rates of the reaction can be assumed to be independent of the concentration of $NaBH_4$, which can be considered as a constant throughout the entire process of the reaction. Because the kinetics of this reaction can be treated as pseudofirst-order to 4-NP concentration, the kinetic equation of the reduction can be written as:[44]

$$- dC_t/dt = dA_t/dt = kC_t t = kA_t t \quad (1)$$

$$\text{or } \ln(C_t/C_0) = \ln(A_t/A_0) = -kt \quad (2)$$

where C_t and A_t are the concentration and absorbance of 4-NP at 400 nm at time t, C_0 and A_0 are the initial concentration and absorbance of 4-NP at 400 nm and k is the apparent rate constant. The plot of $\ln(C_t/C_0)$ against t should give a straight line with slop k. As shown in Fig. 7f, the k for 230 nm, 320 nm, 450 nm and 800 nm are 4.5×10^{-3}, 3.8×10^{-3}, 2.8×10^{-3} and 1.8×10^{-3} s^{-1}, respectively, suggesting that with the size of Ni/SiO_2 MHMs increasing, the catalytic activity and efficiency are lower. However, the rate constant k is not entirely reasonable to compare different supported catalysts because the loading amount is different. Therefore, the turnover frequency (TOF), defined as moles (or numbers) of the product molecules generated per moles (or number) of the catalyst surface atoms was introduced.[45] The dispersion can be calculated based on the diameter of Ni NPs, which is shown in Fig. S4. It can be written as:[46]

$$\text{Dispersion} = 5.03/r \quad (3)$$

Where r is the radius (0.1 nm) of the Ni NPs (detailed deduction process is presented in ESI). And Table 2 displays the dispersions and TOF values of Ni/SiO_2 MHMs with different sizes. Obviously, it shows the consistent trend that is the smaller the size of Ni/SiO_2 MHMs, the higher the catalytic activities. It is worth noting that the catalytic activity of Ni/SiO_2 MHMs with 230 nm is higher than most of the supported Ni NPs.[8,47–53]

Table 2 Rates of reaction and turnover frequencies (TOF) for the reduction of 4-NP by Ni/SiO_2 MHMs with different size.

Sample	Rate constant k [s^{-1}]	Ni loading[a] [wt%]	Ni dispersion [%]	TOF[b] [s^{-1}]
230 nm Ni/SiO_2	4.5×10^{-3},	14.6	8.9	3.4×10^{-3}
320 nm Ni/SiO_2	3.8×10^{-3}	16.4	8.2	2.7×10^{-3}
450 nm Ni/SiO_2	2.8×10^{-3}	13.2	9.3	2.2×10^{-3}
800 nm Ni/SiO_2	1.8×10^{-3}	14.4	4.8	2.0×10^{-3}

[a] Estimated by ICP-AES. [b] Reaction condition: 0.005M 4-NP, 100 μL; 0.01 M $NaBH_4$, 1.0 mL and duration 1 min. Dispersion was calculated based on average Ni NPs in Fig. S4.

The small size and high dispersion of Ni NPs together with high specific surface area of silica support can contribute to it. In addition, the magnetic property makes Ni/SiO_2 MHMs very easy for separation. Notably, the catalyst exhibits excellent catalytic activity even after 10 consecutive cycles of magnetic separation and reduction (Fig. 8). And ICP data for 230 nm Ni/SiO_2 MHMs before and after reaction (Table S2) suggests that there is few Ni NPs leaching after magnetic separation. The well stability can be attributed to the unique *in situ* decomposition and reduction process, which makes the tiny Ni NPs attach on the supports very firmly.

Ni/SiO_2 nano-composite through wet impregnation method

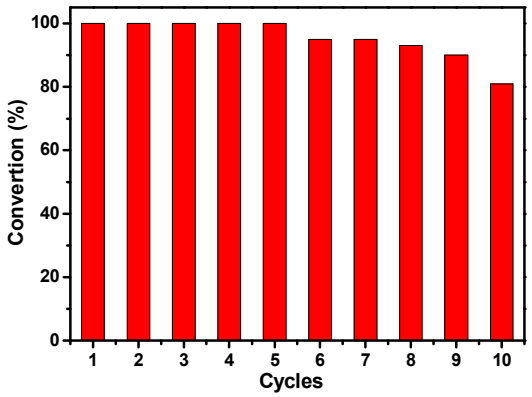

Fig. 8 The reusability of Ni/SiO_2 MHMs as a catalyst for the reduction of 4-NP with $NaBH_4$.

Sample	Type	Average size of nanoparticles (nm)	BET surface area (m^2/g)	κ ($\times10^{-3}$ mg^{-1} s^{-1})	Reference
230 nm Ni/SiO_2 MHMs	Hollow sphere	13.0	185	1.5	This work
320 nm Ni/SiO_2 MHMs	Hollow sphere	12.4	177	1.3	This work
450 nm Ni/SiO_2 MHMs	Hollow sphere	10.5	111	0.9	This work
800 nm Ni/SiO_2 MHMs	Hollow sphere	21.0	65	0.6	This work
Ni/SiO_2 (wet impregnation)	Sphere	20-60	20	0.09	This work
Ni NPs (calcination)	Irregular shape	N/D	15	0.06	This work
Ni@SiO_2	Core-shell	60	223	0.94	[49]
CuNi	Nanocrystals	5	N/D	2.4	[56]
RANEY® Ni	Nanoparticles	Micron-sized	N/D	0.11	[53]
Modified Ni	Nanoparticles	75	35.6	0.83	[53]
RGO/Ni	nanosheet	2-4	N/D	0.04	[8]
Flower-like Ag	Mesostructures	215	N/D	752	[57]
Au@meso-SiO_2	Hollow spheres	15	537	208	[58]
Fe_3O_4@SiO_2-Au@mSiO_2	Core-shell	12.2	256	105	[59]
Ag-C	Nanospheres	10	219	3.4	[60]

N/D: not defined.

Table 3 Comparison of the activity parameter κ of composite Ni catalysts and noble catalysts of similar architecture for the reduction of 4-NP.

and Ni NPs synthesized by calcination and reduction of $Ni(NO_3)_3$ were synthesized for comparison. The TEM images of them are displayed in Fig. S6. It reveals that the average size of Ni NPs obtained by wet impregnation have a large size distribution ranging from 20 nm to 70 nm. And Ni NPs obtained directly through calcination and reduction exhibit irregular shape due to the agglomeration. And the UV-vis spectra of the catalytic reduction of 4-NP to 4-AP developed at different reaction times over Ni/SiO_2 synthesized through wet impregnation method and bare Ni NPs are displayed in Fig. S7. The respective activity parameter κ calculated based on the catalyst constant k is 0.09×10^{-4} mg^{-1} s^{-1} and 0.06×10^{-3} mg^{-1} s^{-1}, which are much slower than 1.5×10^{-3} mg^{-1} s^{-1}. In addition, in order to compare the catalytic activities with other noble metal nano-composite of similar architecture, the activity parameter κ defined as the ratio of k (the rate constant) to the loading amounts of catalysts was introduced.[54,55] Table 3 lists the comparison of catalytic activities in our work and other previously reported. It is obvious that Ni/SiO_2 MHMs we prepared show higher catalytic activity than most of nickel catalysts. These data indicates the good catalytic activity of Ni/SiO_2 MHMs. Besides the high BET surface area and small Ni, the hollow structure of SiO_2 support also contributes to the high catalytic performance of Ni/SiO_2 MHMs. Hollow structures of SiO_2 can accelerate the catalytic reaction because Ni NPs dispersed both inside and outside of the SiO_2 which makes the reactant easier get close to the active sites. Therefore, advantages of this synthesized method are hollow structure of SiO_2 support with high BET surface and nearly monodisperse Ni NPs with tiny size could be obtained. Although the catalytic activities of Ag and Au catalysts (e.g. flower-like Ag and Au@meso-SiO_2) with large surface areas exhibit two magnitude higher than that of Ni/SiO_2 MHMs we prepared, the low cost and the perfect magnetic properties of Ni make Ni/SiO_2 MHMs an advisable option for reduction of 4-NP.

Why the smaller of the Ni/SiO_2 MHMs size, the higher of the catalytic activity? It cannot be due to the total nickel loading amount of the samples. In Table S2, the ICP data of Ni/SiO_2 MHMs with different size reveal that the total nickel amount with different size is almost the same. There are two factors to explain it. First, the smaller of the catalyst size, the higher of the specific surface area (Fig. 2 and Table 1), which can make the reactant easier to get close to the active sites because more nanoparticles are exposed to the reactant. The other is the size of Ni NPs. The smaller nickel NPs can provide larger reaction area and more active sites for reduction. Furthermore, it has been reported that a decrease of the particle size introduce an increase in the fraction of low coordination metal sites, which can promote adsorption of the reactants and accelerate the reaction.[61]

4. Conclusions

In summary, we have synthesized a series of Ni/SiO_2 MHMs with different size (230 nm to 800 nm) by a facile and rational strategy, which is *in situ* decomposition and reduction of silicate precursors. The as-synthesized catalysts possess good catalytic activity, low cost compared with noble metal catalysts and have well stability for recycling. The effects of size of Ni/SiO_2 MHMs for catalytic activity have been investigated. And we find small Ni/SiO_2 MHMs have larger specific surface area and smaller size of Ni NPs, resulting in higher catalytic activity. It is anticipated that this kind of supported materials should be popular because the synthetic method is easy and size of nanoparticles can be readily manipulated through a rational catalyst design. Other study of similar SiO_2 supported metal NPs fabricated through this unique *in situ* decomposition and reduction of inorganic silicate precursors is in progress.

Acknowledgements

This work was supported by funding from financial supports from the National Natural Science Foundation of China (NSFC 21271053, 21401032, 51472058), Research Fund for the Doctoral Program of Higher Education of China (20112304110021), Natural Science Foundation of Heilongjiang Province (LC2012C10), Harbin Sci.-Tech. Innovation Foundation (RC2012XK017012), Fundamental Research Funds for the Central Universities of China (HEUCF201403016), Research and Development of Industrial Technology Project of Jilin Province (JF2012C022-4).

Notes and references

a Key Laboratory of Superlight Materials and Surface Technology, Ministry of Education, College of Material Science and Chemical Engineering, Harbin Engineering University, Harbin 150001, P. R. China. E-mail: yangpiaoping@hrbeu.edu.cn
b These authors contributed equally.

c State Key Laboratory of Theoretical and Computational Chemistry, Jilin University, Changchun 130023, P. R. China
E-mail: syb@jlu.edu.cn.

† Electronic Supplementary Information (ESI) available: [XRD patterns and EDS spectrum of nickel silicate precursor, size distribution histogram of the Ni NPs calculated from a single Ni/SiO_2 MHMs with the different size]. See DOI: 10.1039/b000000x/

1 Z. Zhang, C. Shao, P. Zou, P. Zhang, M. Zhang, J. Mu, Z. Guo, X. Li, C. Wang and Y. Liu, *Chem. Commun.*, 2011, **47**, 3906.
2 Y. Lu, J. Yuan, F. Polzer, M. Drechsler and J. Preussners, *ACS Nano*, 2010, **4**, 7078.
3 Z. Li and H. C. Zeng, *Chem. Mater.*, 2013, **25**, 1761.
4 X. Zhang and Z. Su, *Adv. Mater.*, 2012, **24**, 4574.
5 Y. Mei, Y. Lu, F. Polzer, M. Ballauff and M. Drechsler, *Chem. Mater.*, 2007, **19**, 1062.
6 M. H. Rashid and T. K. Mandal, *Adv. Funct. Mater.*, 2008, **18**, 2261.
7 T. Premkumar and K. Geckeler, *Colloid Surface A*, 2014, **456**, 49.
8 Z. Ji, X. Shen, G. Zhu, H. Zhou and A. Yuan, *J. Mater. Chem.*, 2012, **22**, 3471.
9 N. Sahiner, H. Ozay, O. Ozay and N. Aktas, *Appl. Catal. B*, 2010, **101**, 137.
10 S. Bai, X. Shen, G. Zhu, M. Li, H. Xi and K. Chen, *ACS Appl. Mater. Interfaces*, 2012, **4**, 2378.
11 Y. G. Wu, M. Wen, Q. S. Wu and H. Fang, *J. Phys. Chem. C*, 2014, **118**, 6307.
12 M. Raula, M. H. Rashid, S. Lai, M. Roy and T. K. Mandal, *ACS Appl. Mater. Interfaces*, 2012, **4**, 878.
13 S. Senapati, S. K. Srivastava, S. B. Singh and H. N. Mishra, *J. Mater. Chem.*, 2012, **22**, 6899.
14 D. H. Chen and S. H. Wu, *Chem. Mater.*, 2000, **12**, 1354.
15 R. Dasari, D. A. Robinson and K. J. Stevenson, *J. Am. Chem. Soc.*, 2013, **135**, 570.
16 Y. Xia, Y. Xiong, B. Lim and S. E. Skrabalak, *Angew. Chem. Int. Ed.*, 2009, **48**, 60.
17 A. S. K. Hashmi and G. J. Hutchings, *Angew. Chem. Int. Ed.*, 2006, **45**, 7896.
18 J. Guo and K. S. Suslick, *Chem. Commun.*, 2012, **48**, 11094.
19 X. Li, X. Wang, S. Song, D. Liu and H. Zhang, *Chem.- Eur. J.*, 2012, **18**, 7601.
20 S. H. Zhang, S. Li, Gai, F. He, Y. L. Dai, P. Gao, L. Li and Y. J. Chen. *Nanoscale*, 2014, **6**, 7025.
21 Y. Chi, L. Zhao, Q. Yuan, X. Yan, Y. Li, N. Li and X. Li, *J. Mater. Chem.*, 2012, **22**, 13571.
22 Q. Yuan, N. Li, Y. Chi, W. Geng, W. Yan, Y. Zhao, X. Li and B. Dong, *J. Hazard Mater.*, 2013, **254–255**, 157.
23 C. H. Chen, S. F. Abbas, A. Morey, S. Sithambaram, L. P. Xu, H. F. Garces, W. A. Hines and S. L. Suib, *Adv. Mater.*, 2008, **20**, 1205.
24 J. A. Barreto, W. O'Malley, M. Kubeil, B. Graham, H. Stephan and L. Spiccia, *Adv. Mater.*, 2011, **23**, H18.
25 F. Caruso, R. A. Caruso and H. Möhwald, *Science*, 1998, **282**, 1111.
26 J. Hu, M. Chen, X. Fang and L. Wu, *Chem. Soc. Rev.*, 2011, **40**, 5472.
27 Q. Fang, S. Xuan, W. Jiang and X. Gong, *Adv. Funct. Mater.*, 2011, **21**, 1902.
28 R. Jin, S. Sun, Y. Yang, Y. Xing, D. Yu, X. Yu and S. Song, *Dalton Trans.*, 2013, **42**, 7888.
29 X. Song and L. Gao, *J. Phys. Chem. C*, 2008, **112**, 15299.
30 F. He, P. Yang, D. Wang, C. Li, N. Niu, S. Gai and M. Zhang, *Langmuir*, 2011, **27**, 5616.
31 J. Yu, W. Liu and H. Yu, *Cryst. Growth Des.*, 2008, **8**, 930.
32 S. Kubo, R. Demir-Cakan, L. Zhao, R. J. White and M. M. Titirici, *ChemSusChem*, 2010, **3**, 188.
33 B. Fang, J. H. Kim, C. Lee and J. S. Yu, *J. Phys. Chem. C*, 2007, **112**, 639.
34 M. Sasidharan and K. Nakashima, *Acc. Chem. Res.*, 2013, **47**, 157.
35 N. D. Petkovich and A. Stein, *Chem. Soc. Rev.*, 2013, **42**, 3721.
36 M. Luo, Y. Liu, J. Hu, H. Liu and J. Li, *ACS Appl. Mater. Interfaces*, 2012, **4**, 1813.
37 H. J. Kim, K. I. Choi, A. Pan, I. D. Kim, H. R. Kim, K. M. Kim, C. W. Na, G. Cao and J. H. Lee, *J. Mater. Chem.*, 2011, **21**, 6549.
38 H. Yu, J. Yu, S. Liu and S. Mann, *Chem. Mater.*, 2007, **19**, 4327.
39 S. Liu, G. Huang, J. Yu, T. W. Ng, H. Y. Yip and P. K. Wong, *ACS Appl. Mater. Interfaces*, 2014, **6**, 2407.
40 W. Stöber, A. Fink and E. Bohn, *J. Colloid Interface Sci.*, 1968, **26**, 62.
41 Y. Deng, Y. Cai, Z. Sun, J. Liu, C. Liu, J. Wei, W. Li, C. Liu, Y. Wang and D. Zhao, *J. Am. Chem. Soc.*, 2010, **132**, 8466.
42 J. A. Johnson, J. J. Makis, K. A. Marvin, S. E. Rodenbusch and K. J. Stevenson, *J. Phys. Chem. C*, 2013, **117**, 22644.
43 J. Zheng, Y. Dong, W. Wang, Y. Ma, J. Hu, X. Chen and X. Chen, *Nanoscale*, 2013, **5**, 4894.
44 S. Wunder, F. Polzer, Y. Lu, Y. Mei and M. Ballauff, *J. Phy. Chem. C*, 2010, **114**, 8814.
45 J. Lee, J. C. Park and H. Song, *Adv. Mater.*, 2008, **20**, 1523.
46 J. R. Anderson, *Structure of Metallic Catalysts*, Academic Press, 1975.
47 P. Dhokale, H. Yadav, S. Achary and S. Delekar, *Appl. Surf. Sci.*, 2014, **303**, 168.
48 H. Lu, H. Yin, Y. Liu, T. Jiang and L. Yu, *Catal. Commun.*, 2008, **10**, 313.
49 Z. Jiang, J. Xie, D. Jiang, J. Jing and H. Qin, *CrystEngComm*, 2012, **14**, 4601.
50 Y. Yang, Y. Ren, C. Sun and S. Hao, *Green Chem.*, 2014, **16**, 2273.
51 A. Wang, H. Yin, H. Lu, J. Xue, M. Ren and T. Jiang, *Langmuir*, 2009, **25**, 12736.
52 P. Deka, R. C. Deka and P. Bharali, *New J. Chem.*, 2014, **38**, 1789-1793.
53 Z. Jiang, J. Xie, D. Jiang, X. Wei and M. Chen, *CrystEngComm*, 2013, **15**, 560.
54 B. Baruah, G. J. Gabriel and M. J. Akbashev and M. E. Booher, *Langmuir* 2013, **29**, 4225.
55 Q. An, M. Yu, Y. Zhang, W. Ma, J. Guo, C and Wang, *J. Phys. Chem. C*, 2012, **116**, 22432.
56 B. Borah and P. Bharali, *J. Mol. Catal. A-Chem.*, 2014, **390**, 29.
57 M. Xu and Y. Zhang, *Mater. Lett.*, 2014, **130**, 9.
58 J. Chen, Z. Xue, S, Feng, B. Tu and D. Zhao, *J. Colloid. Interface Sci.*, 2014, **429**, 62.
59 Y. H. Deng, Y. Cai, Z. K. Sun, J. Liu, C. Liu, J. Wei, W. Li, C. Liu, Y. Wang and D. Y. Zhao, *J. Am. Chem. Soc.*, 2010, **132**, 8466.
60 B. Guan, X. Wang, Y. Xiao, Y. Liu and Q. Huo, *Nanoscale*, 2013, **5**, 2469.

61 G. A. Somorjai and Y. Li, *Introduction to surface chemistry and catalysis*, John Wiley & Sons, 2010.

Hierarchical Ni nanoparticles supported silica hollow microspheres were synthesized by a unique and simple two-step method. The particle sizes of Ni can be tuned from 10 nm to 21 nm, which are well dispersed with high loading amount (15 wt.%). Excellent catalytic activity in the reduction of 4-nitrophenol can be achieved on the catalysts.